Ann. Geophysicae 14, 786–793 (1996) © EGS – Springer-Verlag 1996

Annales Geophysicae

Shear flow instabilities in the Earth's magnetotail

R. V. Reddy, G. S. Lakhina

Indian Institute of Geomagnetism, Dr Nanabhai Moos Marg, Colaba, Bombay 400005, India

Received: 3 May 1995/Revised: 27 March 1996/Accepted: 12 April 1996

Abstract. Shear flow instability is studied in the Earth's magnetotail by treating plasma as compressible. A dispersion relation is derived from the linearized MHD equations using the oscillating boundary conditions at the inner central plasma sheet/outer central plasma sheet (OCPS) interface and OCPS/plasma-sheet boundary layer (PSBL) interface, whereas the surface-mode boundary condition is used at the PSBL/lobe interface. The growth rates and the real frequencies are obtained numerically for near-Earth ($|X| \sim 10 - 15\ R_E$) and far-Earth ($|X| \sim 100\ R_E$) magnetotail parameters. The periods and wavelengths of excited modes depend sensitively on the value of plasma-sheet half thickness, L, which is taken as $L = 5\ R_E$ for quiet time and $L = 1\ R_E$ for disturbed time. The plasma-sheet region is found to be stable for constant plasma flows unless $M_{A3} > 1.25$, where M_{A3} is the Alfvén Mach number in PSBL. For near-Earth magnetotail, the excited oscillations have periods of 2–20 min (quiet time) and 0.5–4 min (disturbed time) with typical transverse wavelengths of 2–30 R_E and 0.5–6.5 R_E, respectively; whereas for distant magnetotail, the analysis predicts the oscillation periods of ~8–80 min for quiet periods and 2–16 min for disturbed periods.

1 Introduction

Several processes, such as reconnection (Hones, 1979), the collisional or collisionless tearing-mode instability (Galeev *et al.*, 1978; Lakhina and Schindler, 1988) and the Kelvin-Helmholtz (K-H) instability (Russel, 1972; Miura, 1987), have been discussed in the literature to explain the energy transport from the solar wind through the magnetotail and into the ionosphere. The oscillations excited by the K-H instability in the magnetopause boundary layer between the magnetosheath and the magnetosphere (Ong and Roderick, 1972; Boller and Stolov, 1973; Lee *et al.*, 1981; Mishin and Morozov, 1983; Miura, 1987) are considered to be the main source of geomagnetic micropulsations of the range Pc3-Pc5 (Chen and Hasegawa, 1974; Southwood, 1974; Olson and Rostoker, 1978; Wolfe *et al.*, 1980). The K-H instability is also considered to be important for exciting the low-frequency waves in the plasma-sheet boundary layer (PSBL), the region between the central plasma sheet (CPS) and the lobes (McKenzie, 1970, 1971; Lakhina, 1987; Lee *et al.*, 1988).

The high-speed ion flows in the PSBL and in the inner central plasma sheet (ICPS) are found to be important for the low-frequency dynamics of the Earth's plasma sheet (Lui *et al.*, 1983; Huang and Frank, 1986; Eastman *et al.*, 1984, 1985). The high-speed flow bursts usually last for about 10 s, but many flow events persist for as long as a minute. The occurrence rates of high-speed ion flow bursts in the PSBL, the outer central plasma sheet (OCPS) and the ICPS have been found to have a ratio of 4:1:2 for flows of 400–600 km s^{-1}, and 1:0:1 for flows greater than 800 km s^{-1} (Baumjohann *et al.*, 1990). On the other hand, the PSBL is found to be the site of long-lasting intense ion flows ~10^3 km s^{-1} with a typical lifetime of ~15–60 min (Parks *et al.*, 1984; Grabbe and Eastman, 1984).

A variety of magnetic waves ranging from ULF-ELF and including waves with periods of about 2 min were observed in the plasma sheet (Russel, 1972; Tsurutani *et al.*, 1987 and Smith *et al.*, 1990). These waves would cause the oscillation of the plasma sheet and the neutral sheet. McClay and Radoski (1967) predict that the magnetotail has natural resonant frequencies with periods of ~5–30 min, whereas Siscoe (1969) and McKenzie (1970, 1971) predict somewhat shorter periods ranging from about 30 s to 10 min. Lee *et al.* (1988) have calculated periods in the range 3–30 min which are due to the excitation of streaming-sausage and streaming-tearing instabilities in the magnetotail. Recently, Kalra and Lakhina (1994) have studied the shear-flow instability in the ICPS and found that the excited modes have oscillation periods of 2 s–1 min with typical transverse wavelengths of 0.02–1 R_E.

Correspondence to: R. V. Reddy

In this paper we study the shear-flow instability in the PSBL, treating plasma as compressible. Here we employ a four-layer model for the magnetotail which includes the effects of the lobe plasma. This model is an extension of the three-layer model of Kalra and Lakhina (1994). It is expected that taking a fifth layer, e.g. the magnetopause, would probably change the result, as the boundary condition at the magnetopause would involve solar-wind input, which is neglected in the present model. In Sect. 2, we discuss the formation of the problem using a four-layer model with oscillating boundary condition at the ICPS/OCPS and OCPS/PSBL interfaces, and the surface-mode boundary condition at the PSBL/lobe interface, and obtain the dispersion relation. Therefore the waves generated in the PSBL/lobe interface would oscillate between the northern and southern lobes through the ICPS. The numerical analysis of the dispersion relation and the characteristics of the eigenmodes is discussed.

2 Methodology

We consider a four-layer model of the Earth's magnetotail and the plasma in each layer is considered to be compressible. The magnetotail is taken to be symmetric around the $z = 0$ plane. The ICPS is represented between $z = 0$ to $z = \lambda$ and is called Region 1 as shown in Fig. 1, where only the upper part of the tail is shown. The upper layer from $z = \lambda$ to $z = z_0$, denoted by Region 2, represents the OCPS. The layer between $z = z_0$ and $z = L$ of thickness $a\,(=L - z_0)$ is the PSBL and is denoted by Region 3. The region above $z = L$ represents the lobe and is called Region 4. The one-dimensional configuration for the magnetotail can be justified in the sense that x dependence is much weaker than z dependence for the equilibrium field.

The plasma response in the magnetotail is governed by the following ideal MHD equations

$$\frac{\partial \rho}{\partial t} + \nabla\cdot(\rho \mathbf{v}) = 0, \tag{1}$$

$$\rho\left(\frac{\partial \mathbf{v}}{\partial t} + \mathbf{v}\cdot\nabla\mathbf{v}\right) = -\nabla p + \mathbf{J}\times\mathbf{B}, \tag{2}$$

$$\frac{d}{dt}(p\rho^{-\gamma}) = 0, \tag{3}$$

$$\nabla\times(\mathbf{v}\times\mathbf{B}) = \frac{\partial \mathbf{B}}{\partial t}, \tag{4}$$

$$\nabla\times\mathbf{B} = \mu_0\mathbf{J}, \tag{5}$$

$$\nabla\cdot\mathbf{B} = 0, \tag{6}$$

where ρ, $\mathbf{J}$, $\mathbf{v}$, p, $\mathbf{B}$ are the plasma density, current density, bulk flow velocity, plasma pressure and the magnetic field, respectively. Other symbols have their usual meanings. The initial one-dimensional equilibrium configuration is given by $\mathbf{B}_0 = (B_x(z), B_y(z), 0)$, $\mathbf{v}_0 = (v_x(z), v_y(z), 0)$ and $\rho_0 = \rho_0(z)$.

We define $\mathbf{v} = \mathbf{v}_0 + \mathbf{v}'$ and $\mathbf{v}' = \partial\xi/\partial t + \mathbf{v}_0\cdot\nabla\xi$, where ξ is the Lagrangian displacement vector. The subscript

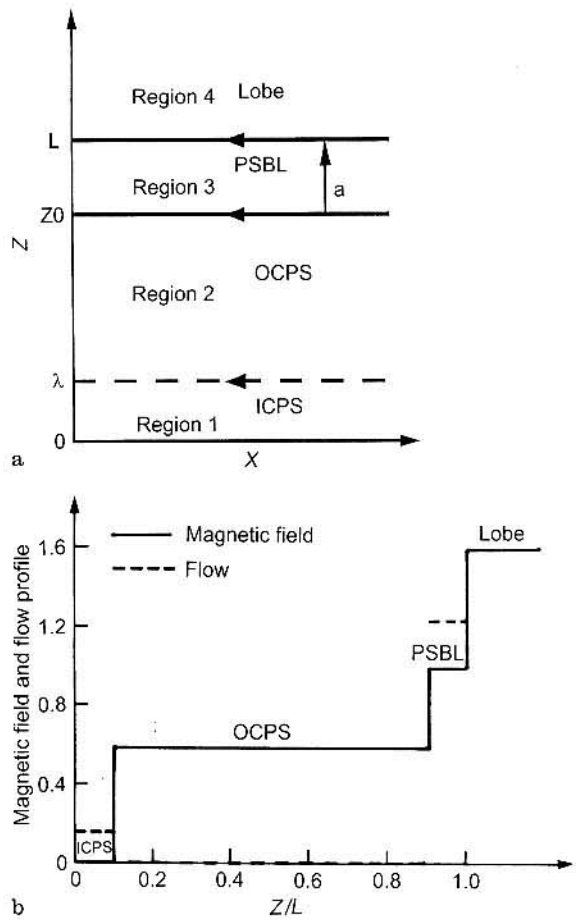

Fig. 1. **a** Schematic of a four-layer model of the Earth's magnetotail. **b** Magnetic and velocity field profiles

0 represents the physical quantities at their equilibrium state, and the prime represents their first order perturbations. By linearizing and assuming perturbations of the form $f' \sim f'(z)exp[i(k_x x + k_y y - \omega t)]$, where $\mathbf{k} = (k_x, k_y, 0)$ and is the wave number, the following wave equation is obtained (Harrold *et al.*, 1990; Kalra and Lakhina, 1994):

$$\frac{\partial}{\partial z}\left(\frac{\varepsilon}{k_\perp^2 - n_0}\frac{\partial \xi_z}{\partial z}\right) = \varepsilon\xi_z, \tag{7}$$

where

$$n_0 = \frac{(v_p^2 - v_a^2)(v_p^2 - c_s^2)k^2}{(c_s^2 + v_a^2)(v_p^2 - c_T^2)}, \quad \varepsilon = \mu_0\rho_0\omega_D^2 - (\mathbf{k}\cdot\mathbf{B}_0)^2,$$

$$k_\parallel = \mathbf{k}\cdot\mathbf{B}_0/B_0, \quad k_\perp = \mathbf{B}_0\times\mathbf{k}/B_0, \quad k = (k_\parallel^2 + k_\perp^2)^{1/2},$$

$$v_a^2 = B_0^2/\mu_0\rho_0, \quad c_T^2 = c_s^2 v_a^2/(c_s^2 + v_a^2),$$

$$v_p = \omega_D/k_\parallel, \quad c_s^2 = \gamma p_0/\rho_0 \quad \text{and} \quad \omega_D = (\omega - \mathbf{k}\cdot\mathbf{v}_0). \tag{8}$$

Equation 7 shows that the perturbed velocity $\mathbf{v}'$, which is connected with the Lagrangian displacement ξ has a component along z. It is singular at the points $\varepsilon = 0$ (Alfvén resonance) and at $v_p^2 = c_T^2$ (cusp resonance). In the absence of flow, these resonances can damp the waves by

resonance absorption and the plasma becomes heated. Further, these resonances give rise to continuum spectrum (Uberoi, 1972). The effects of shear flow on the Alfvén and cusp resonances in the magnetopause current layer have been discussed recently by Parhi and Lakhina (1993, 1994). In the present analysis we avoid these singularities. We consider the plasma density, temperature and magnetic field to be constant but different in each region.

We find that the total perturbed pressure, δp, where $\delta p = \mu_0 P' + \mathbf{B}' \cdot \mathbf{B}_0$ in each region, can be expressed as (Kalra and Lakhina, 1994)

$$\delta p_i = \frac{\mu_0 \rho_{0i}(v_{pi}^2 - v_{ai}^2)k_\parallel^2}{(k_\perp^2 - n_{0i})} \frac{d\xi_i}{dz}, \quad i = 1, 2, 3, 4. \tag{9}$$

For uniform density and magnetic field and constant velocity in Regions 1, 2 and 4, the solutions of Eq. 7 are given by

$$\xi_1 = A_{11} e^{k_1 z} + A_{12} e^{-k_1 z}, \tag{10}$$

$$\xi_2 = A_{21} e^{k_2 z} + A_{22} e^{-k_2 z}, \tag{11}$$

$$\xi_4 = A_4 e^{-k_4 z}, \tag{12}$$

where $k_i = \sqrt{(k_\perp^2 - n_{0i})}$, $i = 1, 2, 4$. The subscripts on ξ and k denote the respective regions, and A_{11}, A_{12}, A_{21}, A_{22} and A_4 are constants. For k_4 real and positive Sol. 12 defines a surface wave perturbation at the PSBL/lobe interface which decreases exponentially in the lobe region. The parameters k_1 and k_2 can be complex quantities, so that the solutions given by ξ_1 and ξ_2 are oscillatory, thus allowing the exchange of energy from one region to another. The matching conditions at the interfaces for such solutions is called as oscillating boundary conditions.

Assuming the PSBL region to be thin, i.e. $ak \ll 1$, integration of Eq. 9 in Region 3 yields

$$\xi_3 = A_{32} + A_{31} \int_{z_0}^{z} dz \frac{(k_\perp^2 - n_{03})}{\mu_0 \rho_{03} k_\parallel^2 (v_{p3}^2 - v_{a3}^2)}, \tag{13}$$

where A_{31}, A_{32} are constants. The above solution for ξ_3 holds good for arbitrary profiles of number density, magnetic field and flow velocity in the PSBL.

2.1 Boundary conditions

The following boundary conditions would complete the problem

$$\xi_3 = \xi_4|_{z=z_0+a}, \quad \delta p_3 = \delta p_4|_{z=z_0+a}, \quad \xi_3 = \xi_2|_{z=z_0},$$

$$\delta p_3 = \delta p_2|_{z=z_0}, \quad \xi_1 = \xi_2|_{z=\lambda} \quad \text{and} \quad \delta p_1 = \delta p_2|_{z=\lambda}. \tag{14}$$

The parity condition:

$$\frac{d\xi_1}{dz} = 0|_{z=0}.$$

Physically, the boundary conditions ensure the continuity of ξ and δp at the interfaces between Regions 1 and 2, and Regions 3 and 4. The parity condition imposes a restriction on the mode structure, i.e. it allows only symmetric solutions.

2.2 The dispersion relation

Even for linear profiles for magnetic field and flow velocity, the solution obtained from Eq. 13 is quite complicated. Therefore, as an initial step we consider constant profile for number density, magnetic field and the flow velocity in Region 3. Under the assumption of $\alpha \ll 1$, where $\alpha = 2k_\parallel v_a c_s / k(c_s^2 + v_a^2)$, and for the velocity profile $v_0(z) = v_0 =$ constant but different in each region, Eq. 13 gives

$$\xi_3 = A_{32} + \frac{A_{31}[k^2(c_{s3}^2 + v_{a3}^2) - \omega_D^2](z - z_0)}{\mu_0 \rho_{03} k_\parallel^2 (c_{s3}^2 + v_{a3}^2)(v_{p3}^2 - v_{a3}^2)}. \tag{15}$$

By using Sols. 10–12 and applying the boundary conditions given by Eq. 14, we obtain the dispersion relation as

$$\frac{\mu_0 \rho_{03}(c_{s3}^2 + v_{a3}^2)(\omega_{D3}^2 - k_\parallel^2 v_{a3}^2)}{[k^2(c_{s3}^2 + v_{a3}^2) - \omega_{D3}^2] - \omega_{D3}^2} - \frac{a l_1(\mu_0 \rho_{04} \omega_{D4}^2 - k_\parallel^2 B_{04}^2)}{[l_2(\mu_0 \rho_{04} \omega_{D4}^2 - k_\parallel^2 B_{04}^2) - k_4 l_1]} = 0, \tag{16}$$

where

$$l_1 = \frac{\mu_0 \rho_{02}(\omega_{D2}^2 - k_\parallel^2 v_{a2}^2)}{k_2 e^{k_2 z_0}} \times \left[\frac{e^{2k_2(z_0 - \lambda)}[k_2 \rho_{01}(\omega_{D1}^2 - k_\parallel^2 v_{a1}^2)\tanh(k_1 \lambda) + k_1 \rho_{02}(\omega_{D2}^2 - k_\parallel^2 v_{a2}^2)]}{k_2 \rho_{01}(\omega_{D1}^2 - k_\parallel^2 v_{a1}^2)\tanh(k_1 \lambda) - k_1 \rho_{02}(\omega_{D2}^2 - k_\parallel^2 v_{a2}^2)} + 1 \right]$$

and

$$l_2 = \frac{1}{e^{k_2 z_0}} \left[1 - \frac{e^{2k_2(z_0 - \lambda)}[k_2 \rho_{01}(\omega_{D1}^2 - k_\parallel^2 v_{a1}^2)\tanh(k_1 \lambda) + k_1 \rho_{02}(\omega_{D2}^2 - k_\parallel^2 v_{a2}^2)]}{k_2 \rho_{01}(\omega_{D1}^2 - k_\parallel^2 v_{a1}^2)\tanh(k_1 \lambda) - k_1 \rho_{02}(\omega_{D2}^2 - k_\parallel^2 v_{a2}^2)} \right].$$

Under the following assumptions, $\omega_{Di}^2 \ll k^2(c_{si}^2 + v_{ai}^2)$, $i = 1, 2, 4$, k_i $(i = 1, 2, 4)$ tends to k, and from Eq. 16 we get the dispersion relation, a polynomial of 8th degree in ω with complicated coefficients given in the Appendix. In the lobe region, plasma density is very low, so that the Alfvén speed V_{A4} becomes very high. In the case of V_{A4} tending to infinity ($\rho_{04} \to 0$), the dispersion relation reduces to a sixth-degree polynomial,

$$F_1 \omega^6 + F_2 \omega^5 + F_3 \omega^4 + F_4 \omega^3 + F_5 \omega^2 + F_6 \omega + F_7 = 0, \tag{17}$$

where

$$F_1 = -k_\parallel^2 \sum_{i=1}^{2} \left(D + \frac{B_{04}^2}{\mu_0 \rho_{03}} \right) X_i, \tag{18}$$

$$F_2 = 2k_\parallel^3 \sum_{i=1}^{2} \left(D + \frac{B_{04}^2}{\mu_0 \rho_{03}} \right) (v_{0i} + v_{02} + v_{03}) X_i, \tag{19}$$

$$F_3 = -k_\parallel^4 \sum_{i=1}^{2} \left\{ \left[\left(D + \frac{B_{04}^2}{\mu_0 \rho_{03}} \right) (B_i + 4v_{0i}(v_{02} + v_{03}) + B_2 + 4v_{02}v_{03}) + \frac{B_{04}^2}{\mu_0 \rho_{03}} (v_{a3}^2 - akD) + DB_3 \right] X_i - D \left[\frac{B_{04}^2}{\mu_0 \rho_{02}} \right] Y_i \right\}, \tag{20}$$

$$F_4 = 2k_\parallel^5 \sum_{i=1}^{2} \left\{ \left[\left(D + \frac{B_{04}^2}{\mu_0 \rho_{03}} \right) (B_i(v_{02} + v_{03}) + B_2(v_{0i} + v_{03}) + 4v_{0i}v_{02}v_{03}) + (v_{0i} + v_{02}) \left(DB_3 + \frac{B_{04}^2}{\mu_0 \rho_{03}} (v_{a3}^2 - akD) \right) \right] X_i + D \left[(v_{0i} + v_{03}) \frac{B_{04}^2}{\mu_0 \rho_{02}} \right] Y_i \right\}, \tag{21}$$

$$F_5 = -k_\parallel^6 \sum_{i=1}^{2} \left\{ \left[\left(D + \frac{B_{04}^2}{\mu_0 \rho_{03}} \right) (B_i(B_2 + 4v_{02}v_{03}) + 4B_2 v_{0i}v_{03})(B_i + B_2 + 4v_{0i}v_{02}) \times \left(DB_3 + \frac{B_{04}^2}{\mu_0 \rho_{03}} (v_{a3}^2 - akD) \right) \right] X_i - D \left[\frac{B_{04}^2}{\mu_0 \rho_{02}} (B_i + 4v_{0i}v_{03} + B_3) \right] Y_i \right\}, \tag{22}$$

$$F_6 = 2k_\parallel^7 \sum_{i=1}^{2} \left\{ \left[\left(D + \frac{B_{04}^2}{\mu_0 \rho_{03}} \right) B_i B_2 v_{03} + (B_i v_{02} + B_2 v_{0i}) \left(DB_3 + \frac{B_{04}^2}{\mu_0 \rho_{03}} (v_{a3}^2 - akD) \right) \right] X_i - D \left[\frac{B_{04}^2}{\mu_0 \rho_{02}} (B_i v_{03} + B_3 v_{0i}) \right] Y_i \right\}, \tag{23}$$

$$F_7 = k_\parallel^8 \sum_{i=1}^{2} \left\{ \left[\frac{B_{04}^2}{\mu_0 \rho_{03}} (B_i B_2 (DB_3 - (v_{a3}^2 - akD))) \right] X_i + D \left[\frac{B_{04}^2}{\mu_0 \rho_{02}} B_i B_3 \right] Y_i \right\}, \tag{24}$$

and

$$X_1 = \tanh(k\lambda)(e^{-2k\lambda} + e^{-2kz_0}), \quad X_2 = \frac{\rho_{02}}{\rho_{01}} (e^{-2k\lambda} - e^{-2kz_0}),$$

$$Y_1 = \tanh(k\lambda)(e^{-2k\lambda} - e^{-2kz_0}), \quad Y_2 = \frac{\rho_{02}}{\rho_{01}} (e^{-2k\lambda} + e^{-2kz_0}),$$

$$B_i = (v_{0i}^2 - v_{ai}^2), \quad D = \frac{k}{ak_\parallel^2} (v_{a3}^2 + c_{s3}^2).$$

The dispersion relation Eq. 17 is solved numerically for different magnetotail parameters. The velocity in Region 2, i.e., v_{02} is taken to be zero.

In Figs. 2–6, we have shown the variation of real frequency (dotted curve) and growth rates (solid curves) normalized with v_{a3}/L versus kL, the normalized wave number. We have given only one curve for real frequency in each figure, because for the parameters of that figure the real frequencies of the unstable modes are more or less the same. We notice from Fig. 2 that the growth rates increase with increasing Mach number M_{Ai} ($M_{Ai} = v_{0i}/v_{a3}$) (cf. solid curves 1–4). The critical value of M_{A3} is 1.25, below which there are no growing modes.

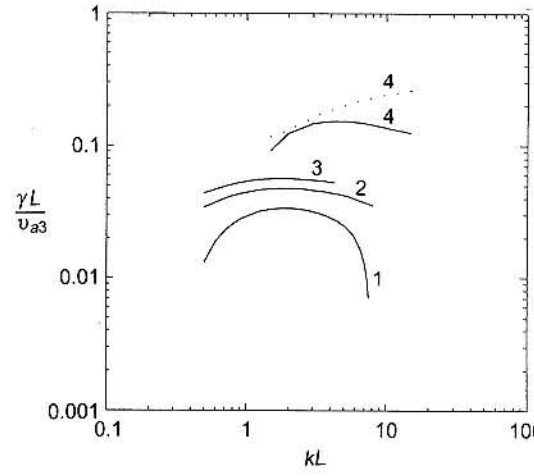

Fig. 2. Variation of growth rates and real frequencies normalized by v_{a3}/L versus the normalized wave number, kL for $\rho_{01}/\rho_{03} = 8.0$, $\rho_{02}/\rho_{03} = 2.5$, $B_{04}/B_{03} = 1.6$, $B_{02}/B_{03} = 0.6$, $\lambda/L = 0.1$, (a/L, z_0/L) = (0.1, 0.9), $k_\parallel L = 0.5$, $M_{A1} = 0.1$, and for $M_{A3} = 1.25$, 1.30 and 1.35 for curves 1, 2 and 3, respectively. Curve 4 is for $M_{A3} = 1.25$ and $M_{A1} = 0.75$. Here, as well as in the remainder of the figures, the *solid* and the *dotted curves* represent growth rates and real frequencies, respectively. Also it should be noted that in Figs. 2–6, only one curve for the real frequency is shown, as all the real frequencies are more or less the same in each figure

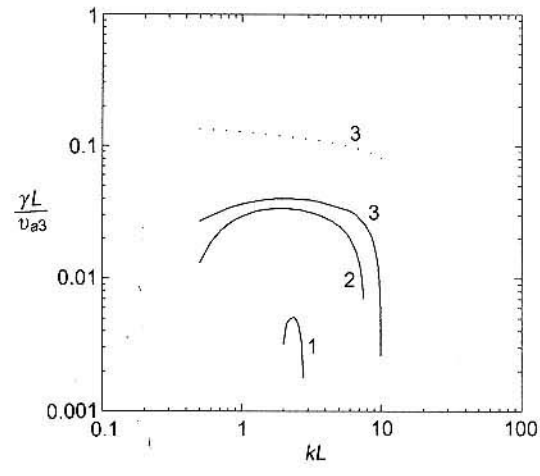

Fig. 3. Same as Fig. 2 but for $M_{A1} = 0.1$, $M_{A3} = 1.25$, and for $\rho_{02}/\rho_{03} = 1.5$, 2.5 and 3.5 for curves 1, 2 and 3, respectively

Figure 3 shows that increasing density ratio ρ_{02}/ρ_{03} results in an increase in growth rates and the shift of unstable wave numbers to higher values of k (cf. solid curves 1–3).

From Fig. 4 it is seen that the growth rates increase with increasing $k_\parallel$. Figure 5 shows the growth curves for

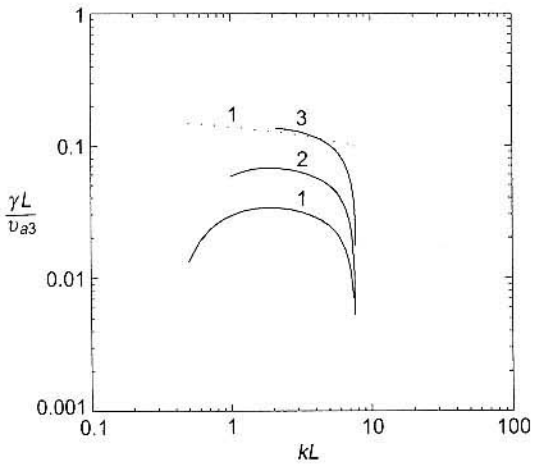

Fig. 4. Same as Fig. 2 but for $M_{A1} = 0.1$, $M_{A3} = 1.25$, and for $k_\parallel L = 0.5$, 1.0 and 2.0 for curves 1, 2 and 3, respectively

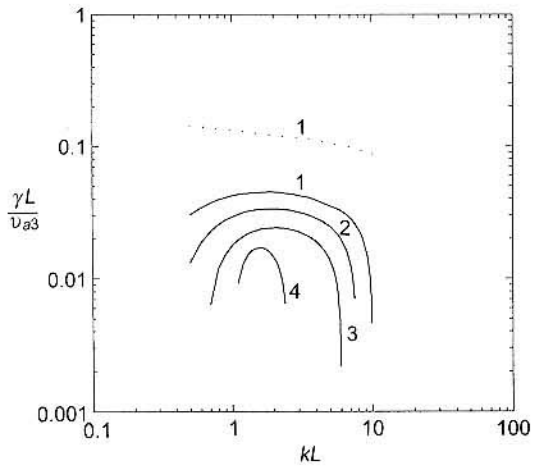

Fig. 5. Same as Fig. 2 but for $M_{A1} = 0.1$, $M_{A3} = 1.25$, $B_{02}/B_{03} = 0.6$, and for $B_{04}/B_{03} = 1.2$, 1.6 and 2.0 for curves 1, 2 and 3, respectively. Curve 4 is for $B_{04}/B_{03} = 1.6$, and $B_{02}/B_{03} = 0.8$

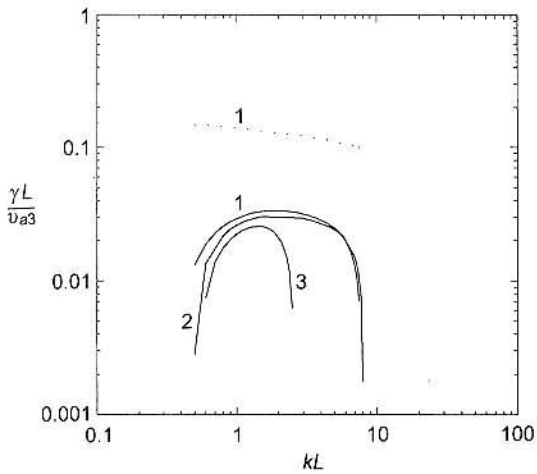

Fig. 6. Same as Fig. 2 but for $M_{A1} = 0.1$, $M_{A3} = 1.25$, $(a/L, z_0/L) = (0.1, 0.9)$ and for $\lambda/L = 0.1$ and 0.3 for curves 1 and 2, respectively. Curve 3 is for $\lambda/L = 0.1$ and $(a/L, z_0/L) = (0.3, 0.7)$

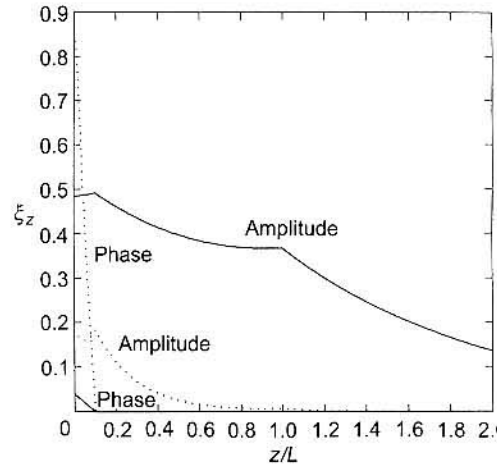

Fig. 7. The solution of the wave equation for the parameters of curve 1 of Fig. 2 using boundary conditions given by Eq. 14. Both the amplitude and phase of ξ_z are shown for $kL = 1$ (*solid curves*) and $kL = 5$ (*dotted curves*)

different values of B_{04}/B_{03} and B_{02}/B_{03}. The growth rates and the range of unstable wave numbers decrease with increasing B_{04}/B_{03}. Similar effect is observed for the variation of B_{02}/B_{03}. From Fig. 6 we notice that the growth rates decrease with increasing λ. The similar effect is noticed for the variation of a, the PSBL thickness. This effect is probably due to the decrease in shear flow scale length in ICPS (or PSBL) as λ (or a) is increased.

Figure 7 shows the variation of normalized ξ_z with z/L for $kL = 1$ (solid curves) and 5 (dotted curves). This figure clearly shows that the mode decays in the lobe and propagates waves to the ICPS. Inside the ICPS, ξ_z develops strong phase modulation.

3 Application

We have applied our analysis separately to both near-Earth and far-Earth magnetotails during quiet and disturbed times.

3.1 Near-Earth magnetotail

For the near-Earth ($|X| \sim 10$–$15\ R_E$) magnetotail, we consider $B_{01} = 0$; $B_{03} = 25$ nT; $n_{03} = 0.2\,\mathrm{cm}^{-3}$ and $T_3 = 1.5$ keV (Lui *et al.*, 1991; Baumjohann, 1993). Accordingly, the Alfvén speed in the ICPS, $v_{a1} = 0$ and in the PSBL $v_{a3} = 1220\ \mathrm{km\,s}^{-1}$. The acoustic speed in the PSBL is $c_{s3} = 400\ \mathrm{km\,s}^{-1}$, and the ion cyclotron frequency, Ω_i, is 2.4 Hz.

For quiet-time magnetotail we have considered the plasma-sheet half thickness as $L = 5\ R_E$ ($1\ R_E = 6370$ km). The predicted real frequencies and growth rates from Figs. 2–6 are $\mathrm{Re}\,\omega \simeq 0.003 - 0.01$ Hz and $\mathrm{Im}\,\omega \simeq 0.0008 - 0.006$ Hz, respectively. The parallel wavelengths for the growing modes are found to be $\lambda_\parallel = 2\pi/k_\parallel \simeq 15$–$60\ R_E$, whereas the transeverse wavelengths are $\lambda_\perp = 2\pi/k_\perp \simeq 2$–$32\ R_E$. The typical periods of the excited modes are ~ 2–20 min.

For the disturbed period of the magnetotail, the typical plasma-sheet half thickness we have considered is $L = 1$ R_E. From Figs. 2–6 it is found that the real frequencies are $\mathrm{Re}\,\omega \simeq 0.015-0.05$ Hz, and the growth rates are $\mathrm{Im}\,\omega \simeq 0.004-0.03$ Hz. The parallel and transverse wavelengths are found to be $\lambda_\parallel = 2\pi/k_\parallel \simeq 3-12\ R_E$ and $\lambda_\perp = 2\pi/k_\perp \simeq 0.5-6.5\ R_E$. The excited oscillations have periods $\sim 0.5-4$ min.

Hence, for same Mach number, the period, as well as the wavelengths of oscillations excited by the shear-flow modes, becomes shorter during disturbed times as compared to the quiet-time conditions.

3.2 *Far-Earth magnetotail*

Observations show that density and temperature in the PSBL more or less remain the same, where as the magnetic field decreases with distance $|X|$ (Baumjohann, 1993). For the distant magnetotail ($|X| = 100\ R_E$) we consider $B_{03} = 5$ nT, $n_{03} = 0.1\ \mathrm{cm}^{-3}$ (Lee *et al.*, 1988). Then, Alfvén speed in the PSBL would be $v_{a3} = 350\ \mathrm{km\,s}^{-1}$ and the ion cyclotron frequency would be $\Omega_i = 0.5$ Hz.

For the quiet-time conditions, Figs. 2–6 predict real frequencies and growth rates to be $\mathrm{Re}\,\omega \simeq 0.0008-0.003$ Hz and $\mathrm{Im}\,\omega \simeq 0.0002-0.002$ Hz respectively. Therefore, the typical periods of the unstable modes are found to be $\sim 8-80$ min, but the unstable wavelengths remain the same as for the near-Earth shear flow modes.

For the disturbed period the real frequencies are found to be $\mathrm{Re}\,\omega \simeq 0.004-0.015$ Hz, while the growth rates are $\mathrm{Im}\,\omega \simeq 0.001-0.01$ Hz. The excited modes have the periods $\sim 2-16$ min.

4 Conclusion

We have considered a one-dimensional configuration of the magnetotail which neglects the curvature of the magnetic field lines. The observations show that the variation of physical parameters are much slower in that x direction as compared to the z direction. Further, the z component of magnetic field, B_{0z}, decreases as tailward distance from the Earth increases. In the far-Earth magnetotail we have $B_{0z} \ll B_0$, and therefore the use of a one-dimensional configuration is justified (Lee *et al.*, 1988). For the near-Earth case the use of one-dimensional magnetotail configuration may be justified during the growth phase of the substorms when $B_{0z} \ll B_0$ (Baumjohann, 1993). The equilibrium flows are usually characterized by v_{0x} and v_{0y} components (Baumjohann *et al.*, 1990; Baumjohann, 1993).

The dispersion relation for shear-flow modes in such an idealized magnetotail consisting of discrete Regions 1–4, representing the ICPS, OCPS, PSBL and lobe, is found to be 8th-degree polynomial in ω with complicated coefficients. For the special case of plasma density in the lobe tending to zero, the dispersion relation for the shear-flow modes reduces to a polynomial of degree six, and this is studied numerically for typical near-Earth and far-Earth parameters of the magnetotail.

Our analysis shows that for the case of near-Earth magnetotail, the modes excited by the shear-flow instabilities would have oscillation periods of 2–20 min (quiet time) and 0.5–4 min (disturbed time) with associated wavelengths (in the dawn-dusk direction) $\sim 2-30\ R_E$ (quiet) and $0.5-6.5\ R_E$ (disturbed). For the case of far-Earth magnetotail, the analysis predicts oscillation periods of $\sim 8-80$ min for quiet time and 2–16 min for disturbed time. The wavelengths of the excited modes are more or less the same as in the near-Earth case. This prediction of theory can be easily tested by the analysis of the data.

We would like to emphasize that the modes considered here are such that they decay in the lobe region going from the PSBL towards the magnetopause, but that the perturbation can propagate from the PSBL to ICPS (cf. Fig. 7 and Eqs. 10–12). Therefore, once excited the shear-flow modes can efficiently exchange energy between Regions 1 and 3. In contrast, the surface-wave modes considered by Kalra and Lakhina (1994) could exist only at the ICPS/OCPS interface. In our case both the shear flows in the ICPS and PSBL regions contribute to the excitement of the unstable modes, which are characterized as body-wave modes in Regions 1 to 3, and as surface-wave type at the PSBL/lobe interface. It is interesting to note that for the symmetric mode (as shown in Fig. 7), ξ_z tends to be maximum at the ICPS/OCPS interface. This can lead to the compression of the ICPS resulting in an intensification of the dawn-dusk current. This enhanced crosstail current may in turn excite some kind of plasma microinstabilities in the neutral sheet (Lui *et al.*, 1991). The microinstabilities could give rise to the anomalous resistivity, which may lead to the substorm onset either by facilitating excitation of the tearing modes or by disruption of the crosstail currents.

For the typical parameters considered here, the shear-flow modes are excited for $M_{A1} = 0.1$ and $M_{A3} = 1.25$. The condition that $M_{A1} = 0.1$ corresponds to $v_{01} \sim 100\ \mathrm{km\,s}^{-1}$ (near-Earth) and $35\ \mathrm{km\,s}^{-1}$ (far-Earth) can be easily satisfied. However $M_{A3} = 1.25$ demands rather a high flow speed in the PSBL region, i.e. $v_{03} \simeq 1500\ \mathrm{km\,s}^{-1}$ (near-Earth) and $450\ \mathrm{km\,s}^{-1}$ (far-Earth). This indicates that the modes discussed here would preferably be excited in the region far from Earth rather than in the near-Earth magnetotail.

These predictions are based on the constant profiles for ρ_0, B_0 and v_0 in Region 3. There is a need to consider realistic profiles for these parameters, as they may affect the eigenmode structure. The analysis is being extended to the case of linear profiles for v_0 and B_0 in Region 3, and the results will be reported elsewhere.

Acknowledgements. Topical Editor K. H. Glaßmeier thanks two referees for their help in evaluating this paper.

Appendix

When $\rho_{04} \neq 0$, the dispersion relation given in Eq. 16 reduces to an eigth-degree polynomial, i.e.

$$C_1\omega^8 + C_2\omega^7 + C_3\omega^6 + C_4\omega^5 + C_5\omega^4 + C_6\omega^3 + C_7\omega^2 + C_8\omega + C_9 = 0, \tag{25}$$

Lee, L. C., R. K. Albano, and J. R. Kan, Kelvin-Helmholtz instability in the magnetopause-boundary layer region, *J. Geophys. Res.*, **86,** 54–58, 1981.

Lee, L. C., S. Wang, C. Q. Wes, and B. T. Tsurutani, Streaming sausage, kink and tearing instabilities in a current sheet with applications to the earth's magnetotail, *J. Geophys. Res.*, **93,** 7354–7365, 1988.

Lui, A. T. Y., T. E. Eastman, D. J. Williams, and L. A. Frank, Observations of ion streaming during substorms, *J. Geophys. Res.*, **88,** 7753–7756, 1983.

Lui, A. T. Y., C. L. Chang, A. Mankofsky, H. K. Wong, and D. Winske, A cross-field current instability for substorm expansions, *J. Geophys. Res.*, **96,** 11389–11401, 1991.

McClay, J. F., and H. R. Radoski, Hydromagnetic propagation in a theta-model geomagnetic tail, *J. Geophys. Res.*, **72,** 4525–4528, 1967.

McKenzie, J. F., Hydromagnetic oscillations of the geomagnetic tail and the plasma sheet, *J. Geophys. Res.*, **75,** 5331–5339, 1970.

McKenzie, J. F., Hydromagnetic wave coupling between the solar wind and the plasma sheet, *J. Geophys. Res.*, **76,** 2958–2965, 1971.

Mishin, V. V., and A. G. Morozov, On the effect of oblique disturbances on Kelvin-Helmholtz instability at magnetospheric boundary layers and in solar wind, *Planet. Space Sci.*, **31,** 821–828, 1983.

Miura, A., Simulation of Kelvin-Helmholtz instability at the magnetospheric boundary, *J. Geophys. Res.*, **92,** 3195–3206, 1987.

Olson, J. V., and G. Rostoker, Longitudinal phase variations of Pc4-5 micropulsations, *J. Geophys. Res.*, **83,** 2481–2488, 1978.

Ong, R. S. B., and N. Roderick, On the Kelvin-Helmholtz instability of the earth's magnetopause, *Planet. Space Sci.*, **20,** 1–10, 1972.

Parhi, S., and G. S. Lakhina, Criteria for shear flow instability in the magnetopause boundary layer region, *Earth Moon Planets*, **62,** 245–258, 1993.

Parhi, S., and G. S. Lakhina, Shear flow instability near the cusp resonance in magnetopause boundary layer, *Earth Moon Planets* **64,** 107–115, 1994.

Parks, G. K., M. McCarthy, R. J. Fitzenreiter, J. Etcheto, K. A. Anderson, R. R. Anderson, T. E. Eastman, L. A. Frank, D. A. Gurnett, C. Huang, R. P. Lin, A. T. Y. Lui, K. W. Ogilvie, A. Pedersen, H. Reme, and D. J. Williams, Particle and field characteristics of the high-latitude plasma sheet boundary layer, *J. Geophys. Res.*, **89,** 8885-8906, 1984.

Russell, C. T., Noise in the geomagnetic tail, *Planet. Space Sci.*, **20,** 1541–1553, 1972.

Siscoe, G. L., Resonant compressional waves in the geomagnetic tail, *J. Geophys. Res.*, **74,** 6482–6486, 1969.

Smith, R. A., M. L. Goldstein, M. R. Sands, R. P. Lepping, C. K. Goertz, B. G. Harrold, C. A. Fitch, and L.-H. Shan, Ultra-low-frequency wavepower in the magnetotail lobes. 1. Relation to substorm onsets and the auroral electrojet index, *Geophys. Res. Lett.*, **17,** 1845–1848, 1990.

Southwood, D. J., Some features of field line resonances in the magnetosphere, *Planet. Space Sci.*, **22,** 483–491, 1974.

Tsurutani, B. T., M. E. Burton, E. J. Smith, and D. E. Jones, Statistical properties of magnetic-field fluctuations in the distant plasma sheet, *Planet. Space Sci.*, **35,** 289–293, 1987.

Uberoi, C., Alfvén waves in inhomogeneous magnetic fields, *Phys. Fluids*, **15,** 1673–1675, 1972.

Wolfe, A., L. J. Lanzerotti, and C. G. Maclennan, Dependence of hydromagnetic energy spectra on solar-wind velocity and interplanetary magnetic-field direction, *J. Geophys. Res.*, **85,** 114–118, 1980.